



ELSEVIER

19 February 2001

Physics Letters A 280 (2001) 129–138

PHYSICS LETTERS A

www.elsevier.nl/locate/pla

Fractal dependence of vector-soliton collisions in birefringent fibers

Jianke Yang*, Yu Tan

Department of Mathematics and Statistics, University of Vermont, 16 Colchester Avenue, Burlington, VT 05401, USA

Received 1 September 2000; received in revised form 18 December 2000; accepted 8 January 2001

Communicated by A.P. Fordy

Abstract

Vector-soliton collisions in birefringent nonlinear optical fibers are investigated. The underlying mathematical model is the non-integrable coupled nonlinear Schrödinger equations. It is shown that the exit velocity versus collision velocity graph has a fractal structure. When we zoom into different positions of this fractal, we get structures which are either a copy, a horizontal reflection or vertical reflection of the original structure. Collision dynamics in the zoomed-in windows and that in the original graph follow simple and well-defined patterns as well. We explain this fractal dependence of the collision by a novel resonance mechanism between translational motion of vector solitons and radiation modes which cause internal oscillations inside a vector soliton. © 2001 Published by Elsevier Science B.V.

1991 MSC: 35Q55; 74J35

Keywords: Vector-soliton collisions; Fractal structure; Resonance

1. Introduction

Solitary wave collisions are common phenomena in physics and engineering. Water wave collisions in the ocean and optical-soliton collisions in wavelength-division-multiplexed fiber transmission systems are well-known examples [1,2]. Solitary wave collisions have been studied extensively for a great variety of nonlinear wave equations in the past four decades. If the equation is integrable, the pioneering work by Zabusky and Kruskal [3] and subsequent developments [1] show that solitary wave collisions are elastic, i.e., they simply pass through each other with-

out change of shape or velocity. However, collisions in non-integrable equations can be much more complex. The most vivid demonstration of this complexity is probably the ϕ^4 model, where kink/antikink collisions depend fractally on the collision velocity [4,5]. The mechanism for this fractal dependence is a resonance between translational motion and internal (shape) modes of kink/antikinks. These internal modes are discrete eigenfunctions (with non-zero eigenvalues) in the linearized ϕ^4 equation expanded around kink/antikink solutions.

In this Letter, we show that a fractal structure can also be created in solitary wave collisions by a resonance between translational motion and *radiation modes* of solitary waves. Since radiation modes exist for all conservative evolution equations, while internal modes exist only for some of them, it is then clear that

* Corresponding author. Tel.: 802-656-4314, fax: 802-656-2552.
E-mail address: jyang@emba.uvm.edu (J. Yang).

our new resonance mechanism for fractal structures is more universal.

The wave system we choose to study is the coupled nonlinear Schrödinger (NLS) equations:

$$iA_t + A_{xx} + (|A|^2 + \beta|B|^2)A = 0, \quad (1.1)$$

$$iB_t + B_{xx} + (|B|^2 + \beta|A|^2)B = 0, \quad (1.2)$$

where A and B are complex amplitudes of wave envelopes, and β is the cross-phase modulational (XPM) coefficient. This system is well known in nonlinear optics. It governs pulse propagation in birefringent fibers [6]. For linearly birefringent fibers, $\beta = 2/3$. For elliptically birefringent fibers, β can take other positive values [7]. Solitary waves in these equations are often called vector solitons in the literature as they generally contain two components. When $\beta = 0$, this system reduces to two separate NLS equations; when $\beta = 1$, the system is called Manakov equations. In both cases, Eqs. (1.1) and (1.2) are integrable [8,9]. Thus vector-soliton collisions are elastic. We note that in the Manakov case, polarization rotation occurs after collision if colliding solitons are not parallelly or orthogonally polarized. But the total intensity and velocity of each vector soliton remains the same [9]. When β is not 0 or 1, these equations are non-integrable. Vector-soliton collisions for the non-integrable case have been studied before in the literature [10–15]. It has been shown that, in addition to passing-through collision, vector solitons can also bounce off each other or trap each other. However, what is still unknown so far is that, this collision can be much more complex and regular at the same time. In this Letter, we will show that, in the non-integrable case, the exit velocity versus collision velocity graph for vector-soliton collisions has a fractal structure. When we zoom into this graph, we can get a copy, a horizontal reflection or vertical reflection of the original graph. Collision dynamics in the zoomed-in windows bears intimate relationships with that in the original graph as well. We explain this fractal structure by a novel resonance mechanism between translational motion of vector solitons and radiation modes which cause internal oscillations inside a vector soliton. Lastly, we show that the experimental verification of these results in birefringent fibers is quite feasible.

2. Fractal structure and its collision dynamics

For simplicity, we only consider the collision of two orthogonally polarized and equal-amplitude vector solitons in this Letter. Such collisions often arise in fiber transmission systems, optical switching and planar waveguides [13,16–18]. The initial conditions for these collisions can be written as

$$A(x, 0) = \sqrt{2} \operatorname{sech}\left(x + \frac{1}{2}\Delta\right) e^{(1/4)iV_0x}, \quad (2.1)$$

$$B(x, 0) = \sqrt{2} \operatorname{sech}\left(x - \frac{1}{2}\Delta\right) e^{-(1/4)iV_0x}, \quad (2.2)$$

where $A(x, 0)$ and $B(x, 0)$ each is a NLS soliton, V_0 is the collision velocity, and Δ ($\gg 1$) is the initial pulse separation. The amplitudes of these colliding solitons have been normalized to be $\sqrt{2}$. Their phases have been removed since Eqs. (1.1) and (1.2) are phase-invariant in both A and B components. We note that for these initial conditions, solutions possess a symmetry: $B(x, t) = A(-x, t)$. When $\beta = 0$ or 1 (integrable case), these two NLS solitons will simply pass through each other without change in amplitude, velocity or polarization. In the Manakov case ($\beta = 1$), polarization rotations do not occur here because the colliding solitons (2.1) and (2.2) are orthogonally polarized [9]. When $\beta \neq 0$ or 1 (non-integrable case), amplitudes, velocities and polarizations of colliding solitons will all change after collision. This non-integrable collision will be the focus of our present study. Throughout this Letter, we choose $\beta = 2/3$, as this is the XPM coefficient for fibers of linear birefringence [6].

We simulated Eqs. (1.1) and (1.2) extensively for initial conditions (2.1) and (2.2), using collision velocity V_0 as a control parameter. The initial pulse separation Δ should be large enough so that the initial pulse overlap is negligible. In our simulations, we used $\Delta = 20$. We employed two different numerical schemes: (1) a third-order split-step method; (2) the pseudo-spectral method coupled with the fourth-order Runge–Kutta integration along time direction. Results of these two schemes were compared closely to guarantee consistency. We also took a large x interval and used damping conditions at its boundaries. These measures were to ensure that radiation emitted into the far field does not interfere with pulse collisions in the center field. In our simulations, the x interval was 160 units wide.

The x -grid points were 1024, and the t -stepsize was 0.01 (split-step method) and 0.004 (pseudo-spectral method). We also ran our simulations on selective V_0 values with longer x intervals, wider initial pulse separations, more grid points and smaller t -stepsize, and were assured that the results did not change. All our simulations used double precision (about 16 significant digits).

Our simulations identified three collision scenarios: transmission, reflection and trapping. In a transmission scenario, most of the energy in each pulse passes through; in a reflection scenario, most of the energy is reflected back; in a trapping scenario, the two pulses trap each other and form a single new pulse. In transmission and reflection scenarios, polarizations of exit pulses generally are rotated to various degrees, a phenomenon called shadow formation in the literature. Exit pulses generally also have a small amount of chirp which decays as pulses escape to the far field (it is noted that chirp causes width and amplitude oscillations to vector solitons). If we define the “exit velocity” V as the difference between velocities of the two exit pulses, then the exit velocity is positive in a transmissional collision, negative in a reflectional collision, and zero in a trapping collision. Numerically, the exit velocity is determined as follows. We let the pulses propagate for a long time after collision. If they still do not separate, we assign the exit velocity as zero. If they do separate, we wait until they have separated far apart and their velocities have stabilized. Then we locate the positions of maximum pulse amplitudes at two different time values. The difference of average velocities of the two pulses in this time interval is assigned as the exit velocity. The sign of the exit velocity is determined by whether most of the pulse energy passes through or is reflected back. In Fig. 1, we show these three collision scenarios for $V_0 = 1.3$, 1.205 and 1.05, respectively. In this figure, only the $|A|$ components are plotted, as the $|B|$ components are simply horizontal reflections of the $|A|$ components due to symmetry $B(x, t) = A(-x, t)$. In Fig. 1(a), the collision is transmissional with exit velocity $V = 0.68$. The two component amplitudes in exit pulses are 1.19 and 0.57, respectively. The collision in Fig. 1(b) is reflectional with $V = -1.01$ and component amplitudes of exit pulses as 1.38 and 0.05. Collision scenario in Fig. 1(c) is trapping. In each collision, some radiation is emitted too.

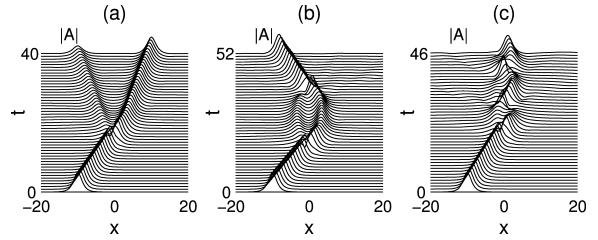


Fig. 1. Three scenarios of vector-soliton collisions: (a) transmission ($V_0 = 1.3$); (b) reflection ($V_0 = 1.205$); (c) trapping ($V_0 = 1.05$). Only $|A|$ components are shown. The $|B|$ components are horizontal reflections of $|A|$.

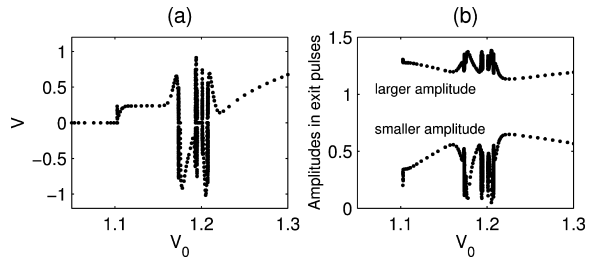


Fig. 2. Collision results for $\beta = 2/3$ with initial conditions (2.1), (2.2) and various collision velocities V_0 : (a) exit velocity V graph; (b) graph of two component amplitudes in exit pulses.

Next, we systematically investigate the collision outcome as the collision velocity V_0 continuously vary. The results are shown in Fig. 2, where the exit velocity and two component amplitudes of exit pulses are plotted in (a) and (b), respectively. As we can see from this graph, when $V_0 \lesssim 1.1024$, the collision is always trapping. When $1.1024 \lesssim V_0 \lesssim 1.1734$ and $V_0 \gtrsim 1.2076$, the collision is always transmissional. But in the interval $1.1734 \lesssim V_0 \lesssim 1.2076$, transmissional, reflectional and trapping collisions all occur in an intertwined way. Notice from Fig. 2(b) that polarizations of initial pulses are clearly rotated after collision. This rotation is generally greater in transmissional collisions than in reflectional collisions.

The surprising feature about Fig. 2 is that, it embeds in itself a fractal structure! To reveal this structure, we will focus on the exit velocity graph Fig. 2(a) in the remainder of this Letter. When we isolate the interval $[1.15, 1.23]$, this graph becomes Fig. 3(a). Our finding is that Fig. 3(a) is a fractal. Before we substantiate this claim, we describe some main features of Fig. 3(a) first. At its left and right ends,

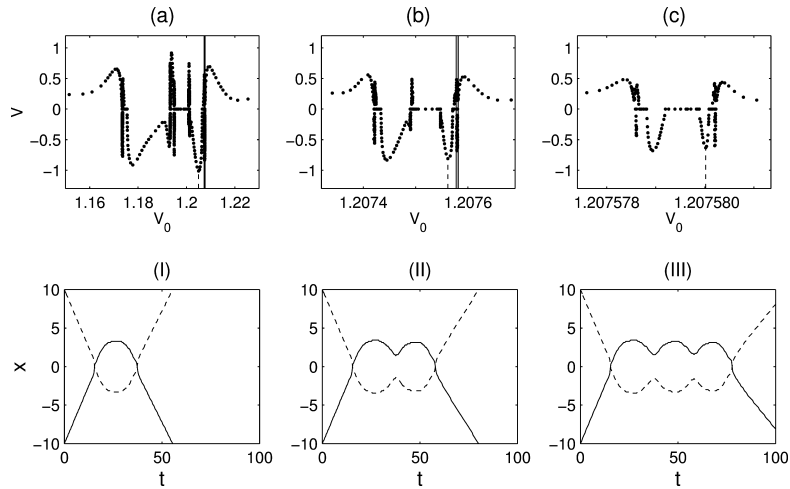


Fig. 3. Fractal structure and collision dynamics of vector solitons. The upper row are graphs of exit velocity V versus collision velocity V_0 . (b) and (c) are successive amplifications of (a) in intervals marked by vertical solid lines. The lower row are collision dynamics of vector solitons with velocities V_0 at bottoms of the N-valleys in the upper row (marked by vertical dashed lines). Specifically, in (I), $V_0 = 1.205$; in (II), $V_0 = 1.207562$; in (III), $V_0 = 1.20758002$. Plotted here are positions of maximum $|A|$ and $|B|$ amplitudes at each time (solid for $|A|$ and dashed for $|B|$).

there are two “hills” where $V > 0$. Between these hills, there are two prominent intervals where $V < 0$ (“valleys”). The left valley is approximately $[1.1755, 1.1932]$, which is wider. We call it the “W-valley”. The right valley, $[1.2013, 1.2065]$, is narrower. We call it the “N-valley”. Between these two valleys, there are even narrower “hills” and “valleys”. In addition, intervals of trapping collisions ($V = 0$) scatter around between these hills and valleys.

To show that Fig. 3(a) is a fractal, we zoom into the tiny V_0 window $[1.20732, 1.20769]$ lying between the N-valley and the right-most hill. This window is marked by two vertical solid lines in Fig. 3(a) (the two lines are so close by that they are almost indistinguishable). This window, when enlarged, is shown in Fig. 3(b). But Fig. 3(b) is qualitatively the same as Fig. 3(a)! In Fig. 3(b), the graph also has two “hills” at the left and right ends. In between, there are also two prominent valleys which are counterparts of the W-valley and N-valley in Fig. 3(a). The W-valley here, $[1.207434, 1.207490]$, is to the left, and the N-valley, $[1.207548, 1.207571]$, is to the right, just like Fig. 3(a). Between these valleys, narrower hills and valleys as well as trapping intervals can be found intertwined too. Some differences also exist between

Figs. 3(a) and (b). The most notable difference is that Fig. 3(b) has less narrower hills and valleys between its W-valley and N-valley. Another difference is that the vertical heights of hills and valleys in Fig. 3(b) are generally lower than their counterparts in Fig. 3(a). But these differences are relatively minor.

The surprise does not stop here. When we zoom into the same relative position in Fig. 3(b) as in Fig. 3(a), we get yet another structure which is similar to Figs. 3(a) and (b). Specifically, we zoom into the narrow interval $[1.2075774, 1.2075814]$, which lies between the N-valley and the right-most hill of Fig. 3(b), the same relative position as the zoomed-in window in Fig. 3(a). This window is marked in Fig. 3(b) by two vertical solid lines. The amplified window is shown in Fig. 3(c). This graph also has two hills at the two ends of the interval. In between, a wider valley is to the left (W-valley), and a narrower valley is to the right (N-valley), just like Figs. 3(a) and (b). These three graphs in Fig. 3 indicate that, the structure in Fig. 3(a) is indeed a fractal! We would like to remind the reader that the length of the V_0 interval in Fig. 3(c) is 4×10^{-6} . On such a fine scale, the collision still has a rich structure, which is truly remarkable. Fig. 3(c) can be zoomed in even

further. But numerical simulations then become more sensitive, and greater accuracy as well as larger initial pulse separation would be required.

What described above is the geometrical structure of the exit velocity graph. Dynamically, we have found that collisions in Fig. 3(a) and its zoomed-in windows (Figs. 3(b) and (c)) are intimately related. Specifically, collisions at the same relative positions in these figures follow simple and clear patterns. To demonstrate, we select the bottom points of N-valleys in these graphs, i.e., $V_0 = 1.205$, 1.207562 and 1.20758002 , respectively (marked in Figs. 3(a)–(c) by vertical dashed lines). In each case, the collision is reflectional ($V < 0$). When we plot the positions of maximum $|A|$ and $|B|$ amplitudes at each time t (solid for $|A|$ and dashed for $|B|$), we get Figs. 3(I)–(III), respectively. In the first graph, Fig. 3(I), the colliding pulses first pass through each other, reach finite separation, stop, return, and pass through each other the second time, and then separate. In Fig. 3(II), the colliding pulses first pass through each other, reach finite separation, stop, oscillate around its position once, then return and pass the second time and separate. In Fig. 3(III), the collision is similar to Figs. 3(I) and (II) except that, the two pulses oscillate twice around their positions between two passes. The clear patterns in these collisions are striking. At other points of the same relative position in Figs. 3(a)–(c), collisions show similar patterns. Specifically, collision in the zoomed-in window is that, after the first pass, the pulses oscillate one more time around their positions than in the original window. The rest of the collision pattern remains the same. We have also observed that time between two passes in Figs. 3(I)–(III) are roughly 21.8, 42.3 and 62.3, respectively. Collision of the same nature as Figs. 3(I)–(III) but with four “bumps” occurs at $V_0 = 1.2075802182$. This point would be the bottom of the next N-valley when we zoom into the narrow window between the N-valley and right-most hill of Fig. 3(c). The time between two passes at this velocity is about 81.1. An interesting fact is that these collision times T_c can be fit nicely by the formula

$$\omega T_c = \delta + 2\pi n, \quad (2.3)$$

where $\omega = 0.316$, $\delta = 0.68$, and n is the number of bumps. The relative error of this fit is less than 1%. Similar relations have been found in kink-antikink

collisions as well [4,5]. In that context, ω was the internal-mode frequency for the kink/antikink.

In Figs. 3(a)–(c), we zoomed into the position between the N-valley and the right-most hill. If we zoom into certain other positions of this fractal (but not any position), we will obtain other types of fine structures. Next, we zoom into the tiny window [1.17324, 1.17385] which lies in Fig. 3(a) between the left hill and the W-valley. For presentation purpose, we copy Fig. 3(a) into Fig. 4(a), then mark this tiny window in Fig. 4(a) by two vertical solid lines. The zoomed-in window is shown in Fig. 4(b). Observe that Fig. 4(b) is just a horizontal reflection of Fig. 4(a)! Here the W-valley, [1.173552, 1.173660], is to the right, and the N-valley, [1.173429, 1.173461], is to the left, just opposite of Fig. 4(a). Dynamically, we found that collisions in the zoomed-in window are also intimately related to those in the original graph. To demonstrate this relationship, we again pick the bottom points of N-valleys in Figs. 4(a) and (b) (this bottom point in Fig. 4(b) is $V_0 = 1.173438$), and plot their collision dynamics in Figs. 4(I) and (II). As we can see, in Fig. 4(II), the two pulses first pass each other and reach finite separation. Then they come back and collide the second time. But they do not pass through each other this time. Instead, they simply separate (bounce off each other), reach finite separation, oscillate around their positions once, collide for the third time, pass through each other, and escape. Comparing the collision in Fig. 4(II) to that in Fig. 4(I), we find that Fig. 4(II) has one more bounce (using the terminology of [4]). In addition, it has one more collision cell (the second piece) in the shape of a double oval. This relationship turns out to be true for collisions anywhere in Fig. 4(a) and its zoomed-in window Fig. 4(b). Specifically, at the same relative positions in these two graphs, the collision in Fig. 4(b) is such that, after the first pass, the two pulses come back and bounce one more time. It is followed by a double-oval-shaped collision cell (see Fig. 4(II)). The rest of the collision is the same as that in Fig. 4(a).

If we zoom into the middle part of Fig. 4(a) between the W-valley and N-valley, we will get a structure which is a vertical reflection of Fig. 4(a). This middle interval, [1.190, 1.202], is marked by two vertical dash-dotted lines in Fig. 4(a). The zoomed-in window is shown in Fig. 4(c). We see that in Fig. 4(c), the “W-valley” and “N-valley” are now upside-down. So

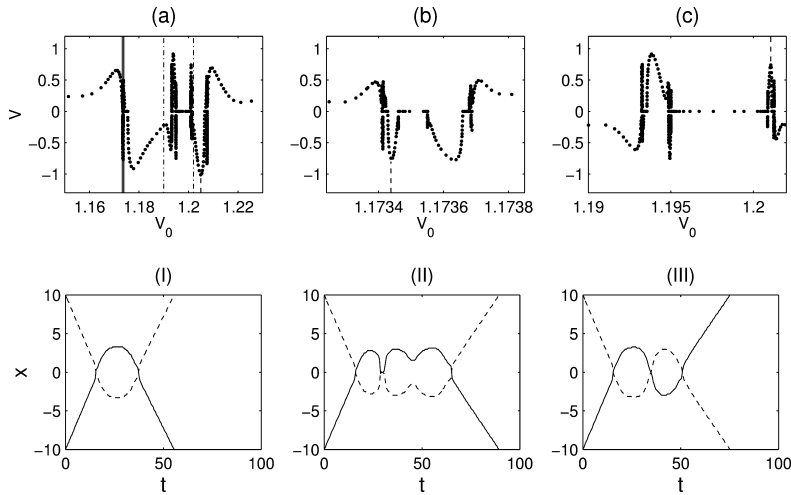


Fig. 4. Fine structures obtained by zooming into two other positions of the fractal in (a). (b) and (c) are the amplifications of the interval in (a) marked by two vertical solid/dash-dotted lines. Lower row are collision dynamics of vector solitons with velocities at the “bottoms” of “N-valleys” in the upper row (marked by vertical dashed lines). Specifically, in (I), $V_0 = 1.205$; in (II), $V_0 = 1.173438$; in (III), $V_0 = 1.201053$. Plotted are positions of maximum $|A|$ and $|B|$ amplitudes at each time (solid for $|A|$ and dashed for $|B|$).

are the “hills” at the two ends of the graph. Note that here “valleys” are not really valleys, and “hills” are not really hills, as they are now upside-down. But we choose to keep using these names so that these structures can be directly related to those in Fig. 4(a). Dynamically, we find that, at the same relative positions in Figs. 4(a) and (c), the collision in Fig. 4(c) is the same as that in Fig. 4(a) except in the end, where instead of escaping, the pulses come back and pass through each other one more time, then escape. An example is shown in Fig. 4(III), where the collision at the “bottom” of the “N-valley” in Fig. 4(c) is plotted. The collision velocity at this bottom is $V_0 = 1.201053$, and it is marked by a vertical dashed line. Compared to Fig. 4(I), pulses in Fig. 4(III) collide one more time in the end, pass through each other, and escape.

The above three zooming operations as shown in Figs. 3(a) and 4(a) are all we found which are non-trivial. Clearly, we can perform any one of these three operations for each graph, and we can do it many times. Do the geometrical and dynamical relationships we have described above between an original graph and its zoomed-in windows persist to all higher zooming operations? Absolutely. To be more specific, whenever we zoom into the position between the N-

valley and its adjacent hill (see Fig. 3(a)), we get a copy of the original graph. Collisions in the zoomed-in window are the same as those at the same relative positions in the original graph, except that toward the end of the collision, the pulses oscillate one more time around their positions (see Figs. 3(I)–(III)). Whenever we zoom into the position between the W-valley and its adjacent hill (see Fig. 4(a)), we get a horizontal reflection of the original graph. Collisions in the zoomed-in window are the same as those at the same relative positions in the original graph, except that toward the end of collision, a double-oval-shaped collision cell is added (see Fig. 4(II)). If we zoom into the position between the W-valley and N-valley, we always get a vertical reflection of the original graph. Collisions in the zoomed-in window follow those at the same relative positions in the original graph, except in the end, where instead of escaping, the pulses come back and pass through each other one more time and escape. We would like to make several remarks here. First, these zooming operations will produce four qualitatively different fine structures altogether. The first one is the original structure as in Fig. 3(a). The second one is its horizontal reflection. The third one is its vertical reflection. The last one is its horizontal and vertical reflection. Second, each zoomed-in window

has its own common collision signature. Furthermore, each point in a window has its own individual collision signature. These collision signatures are generated by zooming operations in the manner we have just described above. Given this collision signature, one can tell where the collision velocity V_0 must be located in the fractal (Fig. 3(a)); conversely, when the location of the collision velocity is specified in this fractal, one can predict the collision dynamics from the above geometrical and dynamical relationships between a graph and its zoomed-in windows. This is analogous to the quadratic map $f(z) = z^2 + c$, where the geometry of its Julia set can be predicted and classified by the location of parameter c in the Mandelbrot set; conversely, the location of c in the Mandelbrot set can be pinpointed by the geometric features of the Julia set [19]. Thirdly, zoomed-in windows may lose certain minor features of the original graph (due to energy radiation, for instance). At high zooming operations, even the W-valley and N-valley can disappear. But if such structures do persist, they must obey the same geometrical and dynamical guidelines as described above.

3. The resonance mechanism

An important question is how to theoretically explain the fractal structure and collision dynamics as seen in Figs. 3 and 4. We notice that collision patterns in Figs. 3(I)–(III) are the simplest, as pulses only collide twice there. Therefore, in this section, we will focus on the theoretical explanation of those collisions. The mechanism responsible for such collisions will be suggestive for more complex collisions such as those in Fig. 4 as well.

Let us first recall that fractal structures in the collision of kinks and antikinks in sine–Gordon type equations have been explained by a resonance between translational motion and internal modes of kink/antikinks [4,5]. Could a similar mechanism be responsible for the present fractal? To answer this question, we examine the collision in Fig. 3(III) in more detail below. The $|A|$ contour of this collision is shown in Fig. 5(a) (the $|B|$ contour is just a horizontal reflection of the $|A|$ contour). We see from this contour plot that after the first pass, each pulse splits into two smaller pulses. Thus roughly speaking, two vector solitons are formed. At $t \approx 26$ (shown in Fig. 5(a) as a horizontal

dashed line), these two solitons reach maximum separation. The $|A|$ and $|B|$ profiles at this time are shown in Fig. 5(b). We have checked the phases of A and B solutions across each pulse span, and found that the phases have a small amount of chirp, but are still close to constants. The small chirp causes weak amplitude and width oscillations inside each vector soliton. Indeed, this oscillation can be seen clearly in Fig. 5(a). It can also be noticed in Fig. 5(c), where the maximum $|A|$ value at each time is plotted. Small oscillations in the lower part of the curve in Fig. 5(c) are due to phase chirps. As these two vector solitons propagate, they are attracted very close to each other, then their individual identities become blurred (this is responsible for large oscillations in Fig. 5(c)). However, the two solitons manage to move away from each other. This process repeats three times until eventually, they collide one last time, pass through each other, and escape. The chirp, or amplitude and width oscillations, in exit pulses is much weaker than that during the collision (see Figs. 5(a) and (c)).

Several oscillations are involved simultaneously in the collision of Fig. 5. One is the oscillation of translational motion of vector solitons as shown in Fig. 3(III). The other one is width oscillations of each vector soliton as discussed above. The third is the oscillation of two-components' relative positions inside a vector soliton. This third oscillation is not specifically shown in Fig. 5. But we have examined the positions of maximum $|A|$ and $|B|$ amplitudes inside each vector soliton, and found that they generally do not coincide with each other. In fact, they oscillate about each other. The oscillational amplitude of this position separation inside a vector soliton is about 0.1. Of these three oscillations, the frequency of the translational motion is $\omega = 0.316$ as in Eq. (2.3). The frequency for width (amplitude) oscillations inside a vector soliton can be inspected from Figs. 5(a) and (c), and it is approximately 0.77. The frequency for positional oscillations inside a vector soliton was numerically determined as about 0.61. We note that these numerical approximations were obtained when the two vector solitons were near their maximal separations. If they are very close to each other, identities of individual vector solitons are ambiguous, thus width and positional oscillations of each vector soliton are not well defined.

Frequencies for width and positional oscillations inside each vector soliton in Fig. 5 can be estimated the-

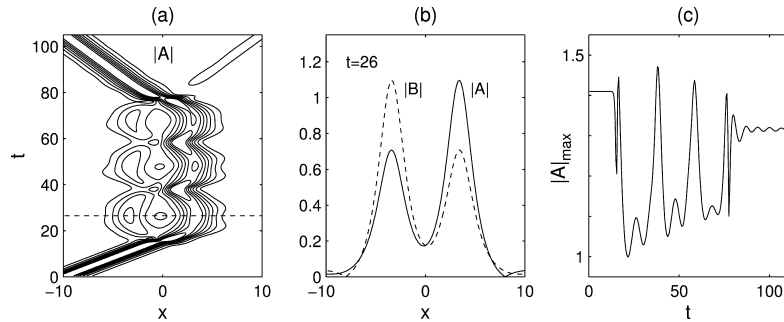


Fig. 5. Detailed collision dynamics of Fig. 3(III) with $V_0 = 1.20758002$. (a) Contour plot of $|A(x, t)|$ at levels 0.2 : 0.15 : 1.1; the horizontal dashed line is at $t = 26$, when the $|A|$ and $|B|$ profiles are shown in (b). (c) Maximum $|A|$ value at each time t .

oretically as well. For this purpose, let us first recall that when a single vector soliton is slightly perturbed, it will undergo positional and width oscillations [20–24]. If this vector soliton supports a discrete internal mode, the eigenvalue of this internal mode will be the frequency of positional oscillations. Otherwise, positional oscillations are caused by quasi-modes which are located inside but close to the edge of the continuous spectrum, and its frequency is about $\min\{\omega_1, \omega_2\}$, where ω_1 and ω_2 are positive propagation constants of the vector soliton [24,25]. Width oscillations are caused by radiation modes, and its frequency is about $\max\{\omega_1, \omega_2\}$. Some of these facts are not obvious. But they can be inferred from the work [26,27] for the single NLS equation, from the work [20] on positional oscillations inside a vector soliton, and from our numerical experiments.

To theoretically estimate width and positional oscillation frequencies in Fig. 5, we assume that these frequencies during the entire collision can be approximated by internal-oscillation frequencies of vector solitons at $t \approx 26$, when the separation of these two vector solitons is maximal. At this instant, the two component amplitudes in each soliton are 1.10 and 0.71, respectively (see Fig. 5(b)). The vector soliton with these amplitude values can be determined uniquely, and its propagation constants are found to be 0.776 and 0.628, respectively [20]. Since polarization angles of these two vector solitons, defined as the arctangent of the amplitude ratios, are about 33° and 57° , these solitons can not support discrete internal modes [21]. Thus the positional oscillation frequency of these solitons is 0.628, and the width oscillational

frequency is 0.776. We see these values are fairly close to those obtained above from numerical inspections.

The important fact we notice is that, both the positional and width oscillation frequencies are fairly close to twice the translational frequency (2ω). This suggests that there is indeed a resonance present in the collision of Fig. 5. This resonance is between the translational motion of vector solitons and positional and width oscillations of each vector soliton. It appears that the positional oscillation frequency is closer to 2ω . So positional oscillation might play a more important role in the resonance mechanism. But Fig. 5 suggests that the resonance with the width oscillation is also significant. Even though the width oscillation frequency does not seem very close to 2ω , we have to bear in mind that when two vector solitons move very close to each other, the resonance dynamics may work a little differently. Thus we have no strong reason to dismiss width oscillations as less important in the collision of Fig. 5. As we have indicated above, both positional and width oscillations in Fig. 5 are caused by radiation modes (quasi-modes is a special case of radiation modes). Thus the resonance here is between the translational motion and radiation modes, rather than discrete internal modes. We have also examined other collisions such as those in Fig. 4, and it seems that the resonance mechanism remains the same. We emphasize that the resonance mechanism in our model is different from that in the ϕ^4 model, where the resonance is between the translational motion and a true localized internal mode [4,5]. Given the fact that radiation modes exist for all conservative evolution equations, while internal modes exist only

for a small number of them, we then expect that more fractal structures may be uncovered where the present resonance mechanism is held responsible. Recently, an interesting Cantor fractal was reported for soliton break-ups due to a sequence of abrupt changes in the dispersion coefficient [28,29]. That fractal is of a different nature as the underlying mechanism is different.

The present Letter only considered collisions of orthogonally polarized and equal-amplitude vector solitons for $\beta = 2/3$. An important question is how this fractal structure changes when colliding vector solitons are not orthogonally polarized, or they do not have equal amplitudes, or β is different from $2/3$. A related question is whether the resonance mechanism of this Letter becomes qualitatively different for other β values or different collision configurations. One other important question is what other physical systems possess fractal structures which are generated by the same resonance mechanism as in this Letter, i.e., a resonance between translational motion and radiation modes of solitary waves. All these questions lie outside the scope of the present Letter. But they will be investigated elsewhere.

Lastly, we discuss the possibility of experimental observation of the fractal structure reported in this Letter. It is known that the dimensionless collision velocity V_0 in our model is related to physical parameters as [6]

$$V_0 = \frac{4\pi \Delta n \tau}{\lambda^2 |D| 1.763}, \quad (3.1)$$

where Δn is the index difference of the fiber's two polarizations, τ is the pulse's full width at half maximum (FWHM), λ is the wavelength, and D is the dispersion parameter (note that D is [6] was defined differently). For step-index single-mode fibers, the typical value for D is 15.6 ps/nm/km at wavelength $\lambda = 1.55 \mu\text{m}$ [30]. According to [31], Δn varies between 5×10^{-9} and 8×10^{-4} . Typical values concentrate in the range 10^{-6} to 10^{-5} . If we let $\tau = 5$ ps, then the total range for V_0 is from 4.8×10^{-3} to 7.6×10^2 , while typical values fall between 0.95 and 9.5. We see that our velocity interval for the fractal structure in Fig. 3(a) falls entirely in the range of typical experimental parameter regime. By fine-tuning the wavelength, one can make V_0 continuously scan over the fractal interval, thus verifying the collision

results experimentally. Of course, experiments are always subject to birefringence fluctuations along the fiber. Thus it may not be very easy to confirm the fractal nature of Fig. 3(a). However, if the two wide reflection valleys (W-valley and N-valley) in Fig. 3(a) can be verified, the resonance mechanism we explained in this Letter will give us confidence that similar structures in zoomed-in windows should also exist. The experimental verification of the W- and N-valleys in Fig. 3(a) should be much easier.

4. Conclusion

In this Letter, we have reported a fractal structure in vector-soliton collisions in birefringent fibers. This structure lies in the exit velocity versus collision velocity graph. We have explained this structure by a resonance mechanism between translational motion of vector solitons and radiation modes which cause internal oscillations inside a vector soliton. These results could have important applications to physical systems where vector-soliton collisions arise. They also have direct ramifications to solitary wave collisions in other physical systems. The experimental confirmation of these results in birefringent fibers is quite feasible.

Acknowledgements

The authors thank Dr. R. Knapp for help with the numerics. We also thank Dr. T.I. Lakoba for helpful discussions. This work was supported in part by AFOSR under contract USAF F49620-99-1-0174 and by NSF under grant DMS-9971712.

References

- [1] M.J. Ablowitz, H. Segur, *Solitons and the Inverse Scattering Transform*, SIAM, Philadelphia, 1981.
- [2] A. Hasegawa, Y. Kodama, *Solitons in Optical Communications*, Clarendon, Oxford, 1995.
- [3] N.J. Zabusky, M.D. Kruskal, *Phys. Rev. Lett.* 15 (1965) 240.
- [4] D.K. Campbell, J.F. Schonfeld, C.A. Wingate, *Physica D* 9 (1983) 1;
D.K. Campbell, M. Peyrard, P. Sodano, *Physica D* 19 (1986) 165.
- [5] P. Anninos, S. Oliveira, R.A. Matzner, *Phys. Rev. D* 44 (1991) 1147.

- [6] C.R. Menyuk, IEEE J. Quantum Electron. QE-23 (1987) 174.
- [7] C.R. Menyuk, IEEE J. Quantum Electron. 25 (1989) 2674.
- [8] V.E. Zakharov, A.B. Shabat, Sov. Phys. JETP 34 (1972) 62.
- [9] S.V. Manakov, Sov. Phys. JETP 38 (1974) 248.
- [10] B.A. Malomed, S. Wabnitz, Opt. Lett. 16 (1991) 1388.
- [11] C. Sophocleous, D.F. Parker, Opt. Comm. 112 (1994) 214.
- [12] J. Yang, D.J. Benney, Stud. Appl. Math. 96 (1996) 111.
- [13] C. Anastassiou, M. Segev, K. Steiglitz, J.A. Giordmaine, M. Mitchell, M. Shih, S. Lan, J. Martin, Phys. Rev. Lett. 83 (1999) 2332.
- [14] J. Yang, Phys. Rev. E 59 (1999) 2393.
- [15] B. Tan, J.P. Boyd, Chaos Solitons Fractals, to appear.
- [16] M.N. Islam, Ultrafast Fiber Switching Devices and Systems, Cambridge University Press, New York, 1992.
- [17] S. Blair, K. Wagner, R. McLeod, Opt. Lett. 19 (1994) 1945.
- [18] N.S. Bergano et al., in: OFC '98, San Jose, CA, 1998, paper PD 12.
- [19] H.O. Peitgen, P.H. Richter, The Beauty of Fractals, Springer, Berlin, 1986.
- [20] J. Yang, Stud. Appl. Math. 98 (1997) 61.
- [21] D.E. Pelinovsky, J. Yang, Stud. Appl. Math. 105 (2000) 245.
- [22] T. Ueda, W.L. Kath, Phys. Rev. A 42 (1990) 563.
- [23] D.J. Kaup, B.A. Malomed, R.S. Tasgal, Phys. Rev. E 48 (1993) 3049.
- [24] B.A. Malomed, R.S. Tasgal, Phys. Rev. E 58 (1998) 2564.
- [25] C. Etrich, U. Peschel, F. Lederer, B.A. Malomed, Yu.S. Kivshar, Phys. Rev. E 54 (1996) 4321.
- [26] M.W. Chbat, P.R. Prucnal, M.N. Islam, C.E. Socolich, J.P. Gordon, J. Opt. Soc. Am. B 10 (1993) 1386.
- [27] E.A. Kuznetsov, A.V. Mikhailov, I.A. Shimokhin, Physica D 87 (1995) 201.
- [28] S. Sears, M. Soljacic, M. Segev, D. Krylov, K. Bergman, Phys. Rev. Lett. 84 (2000) 9.
- [29] M. Soljacic, M. Segev, C.R. Menyuk, Phys. Rev. E 61 (2000) 2.
- [30] G.P. Agrawal, Nonlinear Fiber Optics, Academic Press, San Diego, 1995.
- [31] I.P. Kaminow, IEEE J. Quantum Electron. QE-17 (1981) 15.